Soft Matter

PAPER

View Article Online
View Journal | View Issue

Cite this: *Soft Matter*, 2021, **17**, 5602

Rational synthesis of novel biocompatible thermoresponsive block copolymer worm gels†

Deborah L. Beattie, Oleksandr O. Mykhaylyk, Anthony J. Ryan and Steven P. Armes *

It is well known that reversible addition–fragmentation chain transfer (RAFT) aqueous dispersion polymerization of 2-hydroxypropyl methacrylate (HPMA) enables the rational design of diblock copolymer worm gels. Moreover, such hydrogels can undergo degelation on cooling below ambient temperature as a result of a worm-to-sphere transition. However, only a subset of such block copolymer worms exhibit thermoresponsive behavior. For example, $PMPC_{26}$–$PHPMA_{280}$ worm gels prepared using a poly(2-(methacryloyloxy)ethyl phosphorylcholine) ($PMPC_{26}$) precursor do not undergo degelation on cooling to 6 °C (see S. Sugihara *et al.*, *J. Am. Chem. Soc.*, 2011, **133**, 15707–15713). Informed by our recent studies (N. J. Warren *et al.*, *Macromolecules*, 2018, **51**, 8357–8371), we decided to reduce the mean degrees of polymerization of both the PMPC steric stabilizer block and the structure-directing PHPMA block when targeting a pure worm morphology. This rational approach reduces the hydrophobic character of the PHPMA block and hence introduces the desired thermoresponsive character, as evidenced by the worm-to-sphere transition (and concomitant degelation) that occurs on cooling a $PMPC_{15}$–$PHPMA_{150}$ worm gel from 40 °C to 6 °C. Moreover, worms are reconstituted on returning to 40 °C and the original gel modulus is restored. This augurs well for potential biomedical applications, which will be examined in due course. Finally, small-angle X-ray scattering studies indicated a scaling law exponent of 0.67 (≈2/3) for the relationship between the worm core cross-sectional diameter and the PHPMA DP for a series of PHPMA-based worms prepared using a range of steric stabilizer blocks, which is consistent with the strong segregation regime for such systems.

Received 25th March 2021,
Accepted 10th May 2021

DOI: 10.1039/d1sm00460c

rsc.li/soft-matter-journal

Introduction

Polymerization-induced self-assembly (PISA) enables the highly efficient and convenient preparation of block copolymer nano-objects in the form of concentrated dispersions.[1,2] In view of its remarkable versatility and tolerance of monomer functionality, reversible addition–fragmentation chain transfer (RAFT) polymerization[3–6] has emerged as the most popular synthetic technique for PISA syntheses.[7,8] Thus, if the target diblock composition and other synthesis parameters are optimized, then spherical,[9,10] worm-like[11–13] or vesicular[14,15] morphologies can be produced in various solvents using a wide range of vinyl monomers.[16–22] In particular, PISA *via* RAFT aqueous dispersion polymerization[23–26] is ideally suited for the preparation of nano-objects with potential biomedical applications. Such formulations involve the chain extension of a water-soluble precursor using a water-miscible monomer. The growing second block becomes water-insoluble at some critical degree of polymerization (DP), thus driving *in situ* self-assembly to form sterically-stabilized nanoparticles comprising amphiphilic diblock copolymer chains.

One of the most extensively researched RAFT aqueous dispersion polymerization formulations employs poly(glycerol monomethacrylate) (PGMA) as the hydrophilic steric stabilizer and poly(2-hydroxypropyl methacrylate) (PHPMA) as the hydrophobic core-forming block.[27] PGMA–PHPMA worm gels are of particular interest because they form soft physical gels *via* multiple inter-worm contacts.[27] Such gels are highly biocompatible and exhibit thermoresponsive behavior,[28] undergoing a reversible worm-to-sphere transition on cooling from 20 °C to 4 °C.[29] At a sufficiently high copolymer concentration, this change in morphology results in degelation to produce a free-flowing dispersion at sub-ambient temperature, enabling facile sterilization *via* cold ultrafiltration.[30] Both the critical gelation temperature (CGT) and the worm gel strength can be tuned by statistical incorporation of suitable methacrylic

Dainton Building, Department of Chemistry, University of Sheffield, Brook Hill, Sheffield, South Yorkshire, S3 7HF, UK. E-mail: s.p.armes@shef.ac.uk

† Electronic supplementary information (ESI) available: Assigned ^{1}H NMR spectra; GPC curves; TEM images for $PMPC_{15}$–$PHPMA_{150}$ nano-objects subject to temperature cycling; relationship between sphere and worm core radii; fitted SAXS pattern of $PMPC_{26}$–$PHPMA_{280}$ worms and associated structural parameters; oscillatory rheology strain, angular frequency and time sweeps and X-ray scattering model details. See DOI: 10.1039/d1sm00460c

comonomers or appropriate reactive functional groups (*e.g.* disulfide bonds) into the core or stabilizer blocks, respectively.[31–34] Thus, PGMA–PHPMA worm gels induce human pluripotent stem cell colonies to undergo reversible stasis at 37 °C[35] and can be used in conjunction with poly(vinyl alcohol) for the cryopreservation of red blood cells,[36] while closely-related disulfide-functionalized worm gels provide a convenient 3D cell culture medium for up to ten days.[37] In each case, thermoreversible (de)gelation is a critical feature for the intended biomedical application.

Poly(2-(methacryloyloxy)ethyl phosphorylcholine) (PMPC) is a well-known highly biocompatible zwitterionic polymer[38–45] that has been used to manufacture low-irritation soft contact lenses, coatings for drug-eluting stents and other biomedical devices.[46–51] In 2011 Sugihara *et al.*[15] conducted the RAFT aqueous dispersion polymerization of 2-hydroxypropyl methacrylate (HPMA) using a relatively short PMPC steric stabilizer and obtained well-defined spheres, worms, or vesicles depending on the precise PISA formulation. A pseudo-phase diagram was constructed for a series of $PMPC_{25}$–$PHPMA_x$ diblock copolymers but pure worms and vesicles were only obtained when targeting relatively long PHPMA blocks ($x > 220$). Unfortunately, such higher order nano-objects did not exhibit thermoresponsive behavior, which precludes many potential biomedical applications.

Recently, Warren *et al.*[52] compared the aqueous rheological properties of $PGMA_{37}$–$PHPMA_{80}$, $PGMA_{54}$–$PHPMA_{140}$ and $PGMA_{71}$–$PHPMA_{200}$ worms and found that their thermoresponsive behavior was strongly dependent on the diblock copolymer composition. More specifically, $PGMA_{37}$–$PHPMA_{80}$ worms proved to be unstable with respect to dilution, while a 10% w/w aqueous dispersion of $PGMA_{71}$–$PHPMA_{200}$ worms merely exhibited irreversible degelation on cooling; only the $PGMA_{54}$–$PHPMA_{140}$ worms exhibited the desired thermoreversible (de)gelation at this copolymer concentration. This indicates that such behavior requires careful optimization of the mean DPs of both blocks. Thus, if the DP of the core-forming PHPMA block is too high, then these chains become too hydrophobic to exhibit thermoreversible (de)gelation behavior. Moreover, if the hydrophilic PGMA block is too long, the multiple sphere-sphere fusion that is required for regelation *via* a sphere-to-worm transition is unlikely to occur within a useful experimental timescale (minutes).

In the present study, we revisit the $PMPC_{25}$–$PHPMA_x$ formulation reported by Sugihara *et al.*[15] and target a significantly lower DP of 15 for the hydrophilic PMPC stabilizer block. In principle, this strategy should ensure that the DP required for the hydrophobic PHPMA block to produce a pure worm phase is sufficiently short to produce the desired thermoreversible (de)gelation behavior. The veracity of this rational approach is demonstrated by direct comparison of the aqueous solution properties of such worms with those exhibited by higher molecular weight non-thermoresponsive $PMPC_{26}$–$PHPMA_{280}$ worms (*i.e.* similar to the $PMPC_{25}$–$PHPMA_x$ worm examples previously reported by Sugihara *et al.*).[15] The longer-term aim of this fundamental study is to examine whether such phosphorylcholine-based thermoresponsive worm gels offer potential biomedical applications as new wholly synthetic media for either cell culture[35,36] or cell storage.[37,53]

Experimental

Materials

2-(Methacryloyloxy)ethyl phosphorylcholine (MPC) was purchased from NOF Corporation (Japan) and was used as received. 2-Cyano-2-propyl benzodithioate (CPDB) was purchased from Sigma-Aldrich (Dorset, UK) and 2,2′-azobis(2-methylpropionitrile) (AIBN) was purchased from Molekula (UK). HPMA monomer was kindly provided by GEO Specialty Chemicals (Hythe, UK) and was used as received. 2,2′-Azobis[2-(2-imidazolin-2-yl)propane]dihydrochloride (VA-044) initiator was purchased from Fluorochem (Glossop, UK). Deionized water was used in all experiments and was obtained from an Elgastat Option 3A water purification unit. HPLC-grade chloroform, methanol and ethanol were obtained from VWR Chemicals (UK). Deuterated methanol (CD_3OD) was purchased from Cambridge Isotope Laboratories (UK).

Methods

Synthesis of poly(2-(methacryloyloxy)ethyl phosphorylcholine) (PMPC) precursors *via* RAFT solution polymerization. An example of a typical protocol for the RAFT solution polymerization of MPC is as follows: MPC monomer (3.000 g, 10.2 mmol), CPDB (0.281 g, 1.27 mmol), and AIBN initiator (0.042 g, 0.25 mmol, CPDB/AIBN molar ratio = 5.0) were dissolved in ethanol (4.984 g) to afford a 40% w/w solution in a sample vial. The sealed vial was immersed in ice and the reaction mixture was purged with nitrogen gas for 30 min. The vial was then placed in a stirred oil bath set at 70 °C for 160 min. The polymerization was quenched by cooling to 20 °C and exposing the contents of the flask to air. A final MPC conversion of 79% was determined *via* ^{1}H NMR spectroscopy. The crude PMPC was purified by precipitation (three times) into a ten-fold excess of a 17 : 1 v/v acetone/methanol mixture. Residual solvent was removed under reduced pressure, then the purified PMPC was dissolved in deionized water and freeze-dried overnight to produce a glassy pink solid. ^{1}H NMR spectroscopy analysis indicated a mean degree of polymerization of 15. GPC analysis [refractive index detector, 3 : 1 chloroform/methanol eluent, poly(methyl methacrylate) (PMMA) calibration standards] indicated an M_n of 6300 g mol^{-1} and an M_w/M_n of 1.12.

Synthesis of worm gels *via* RAFT aqueous dispersion polymerization of HPMA. For a typical RAFT aqueous dispersion polymerization of HPMA targeting $PMPC_{15}$–$PHPMA_{150}$ worms at 25% w/w solids, the following protocol was utilized. The $PMPC_{15}$ precursor (0.538 g, 0.12 mmol), HPMA monomer (2.500 g, 17.3 mmol) and VA-044 initiator (9.3 mg, 28.9 μmol, macro-CTA/VA-044 molar ratio = 4.0) were dissolved in deionized water (9.141 g) in a 25 mL round-bottomed flask to afford a 25% w/w solution. The flask was sealed and the solution purged with nitrogen gas for 30 min. Then the flask was placed in a stirred oil bath set at 50 °C for 150 min to ensure high HPMA conversion. The polymerization was

quenched by exposing the flask contents to air while cooling to 20 °C. ^{1}H NMR spectroscopy studies indicated a final HPMA conversion of more than 99%. The $PMPC_{15}$–$PHPMA_{150}$ chains were analyzed by GPC (refractive index detector, 3 : 1 chloroform/methanol eluent, PMMA calibration standards) without further purification (M_n = 29 600 g mol^{-1}; M_w/M_n = 1.30). The $PMPC_{15}$–$PHPMA_{150}$ worms were characterized as a function of temperature using DLS, TEM, SAXS, NMR, rheology and SIPLI.

Characterisation methods

^{1}H NMR spectroscopy. ^{1}H NMR spectra were recorded in CD_3OD at 298 K using a 400 MHz Bruker Avance-400 spectrometer with 64 scans being averaged per spectrum.

Gel permeation chromatography (GPC). All GPC analysis was conducted at 35 °C using a 3 : 1 v/v chloroform/methanol eluent containing 2 mM LiBr at a flow rate of 1.0 mL min^{-1}. The instrument set-up comprised an Agilent 1260 GPC system, two Agilent PL gel 5 μm Mixed-C columns connected in series with a guard column, a refractive index detector and a variable wavelength UV detector set to 308 nm. Calibration was achieved using a series of ten near-monodisperse PMMA standards with M_p values ranging from 625 to 618 000 g mol^{-1}.

Variable temperature dynamic light scattering (DLS). Measurements were performed using a Malvern Zetasizer NanoZS instrument equipped with a 4 mW He–Ne laser (λ = 633 nm) and an avalanche photodiode detector at a fixed scattering angle of 173°. All measurements were recorded on 0.10% w/w aqueous dispersions in disposable cuvettes. An initial cooling cycle from 30 to 6 °C was followed by a heating cycle from 6 to 30 °C, with 5 min being allowed for thermal equilibration at each temperature. The Stokes–Einstein equation was used to calculate the 'sphere-equivalent' *z*-average hydrodynamic diameter, obtained using a non-negative least squares (NNLS) algorithm. Data were averaged over three consecutive runs comprising ten measurements per run.

Transmission electron microscopy (TEM). Dispersions were diluted to 0.10% w/w using deionized water at 6 °C (within a refrigerator) and also 25 °C (within a temperature-controlled oven). Copper–palladium TEM grids were surface-coated in-house with a thin film of carbon before being plasma glow-discharged for 30 s to produce a hydrophilic surface. A 7 μL droplet of a dilute aqueous dispersion of $PMPC_x$–$PHPMA_y$ diblock copolymer nano-objects was deposited onto the surface of each grid (pre-equilibrated at either 6 °C or 25 °C) for 1 min before blotting with filter paper to remove excess liquid. A 7 μL droplet of a 0.75% w/v aqueous uranyl formate solution was then applied as a negative stain for 25 s prior to careful blotting and drying using a vacuum hose. Imaging was performed using a FEI Tecnai Spirit 2 microscope operating at 80 kV and equipped with an Orius SC1000B camera.

Small angle X-ray scattering (SAXS). SAXS patterns were collected using a laboratory-based Xeuss 2.0 beamline (Xenocs, Grenoble, France) equipped with a liquid gallium MetalJet X-ray source (Excillum, Kista, Sweden; λ = 0.134 nm) and a Pilatus 1 M pixel detector (Dectris, Baden, Switzerland). The instrument set-up provided a q range of 0.003 to 0.14 Å^{-1}, where q is the length of the scattering vector (*i.e.* $q = 4\pi\cdot\sin\theta/\lambda$ and θ is one-half of the scattering angle). Measurements were conducted on 1.0% w/w aqueous copolymer dispersions placed within 2.0 mm diameter capillary sample holders. The resulting two-dimensional scattering patterns were calibrated and reduced to one-dimensional curves using Irena SAS macro for Igor Pro.[54]

Oscillatory rheology. Measurements were recorded using an AR-G2 rheometer (TA Instruments, Delaware, USA) set for cone-and-plate geometry (a variable temperature Peltier plate and a 40 mm 2° aluminum cone). The oscillatory mode was utilized to determine the storage modulus (G') and loss modulus (G'') as a function of the strain amplitude, angular frequency, time and temperature. These studies enabled the critical gelation concentration (CGC) and gel strength to be assessed. Strain amplitude sweeps were conducted between 0.1 and 100% at 25 °C using an angular frequency of 1.0 rad s^{-1}. Angular frequency sweeps were conducted between 0.1 and 100 rad s^{-1} at 25 °C using a strain amplitude of 1.0%. To determine the CGC, time sweeps were conducted for 5 min at 10 s intervals by applying a strain amplitude of 1.0% and an angular frequency of 1.0 rad s^{-1}. Cooling and heating thermal cycles were conducted between 40 and 6 °C at 1 °C intervals, allowing 10 min for thermal equilibration at each temperature and using an applied strain of 1.0% and an angular frequency of 1.0 rad s^{-1}.

Shear-induced polarized light imaging (SIPLI). Polarized light images were recorded at various temperatures using a Physica MCR301 mechano-optical rheometer (Anton Paar, Graz, Austria) equipped with a SIPLI attachment and variable temperature Peltier (bottom plate and hood) heaters. A detailed description of this instrument can be found elsewhere.[55,56] A plate–plate geometry consisting of a 25 mm polished steel plate fixture and a fused quartz bottom plate with a fixed gap of 1.0 mm was utilized for these experiments. An angle of 90° between the polarizer and analyzer was employed to obtain polarized light images using a color CCD camera (Lumenera Lu165c). These images were recorded under shear at various temperatures (6, 25 and 37 °C, equilibrated for 10 min at each) for an 18% w/w aqueous dispersion of $PMPC_{15}$–$PHPMA_{150}$ nano-objects or a 10% w/w aqueous dispersion of $PMPC_{26}$–$PHPMA_{280}$ worms using a maximum (sample edge) shear rate of 1.0 s^{-1} applied for 250 s in each case.

Results and discussion

The two-step aqueous PISA synthesis of the two types of PMPC–PHPMA worms examined in this study is outlined in Scheme 1. A dithiobenzoate-based RAFT agent (CPDB) and AIBN initiator were employed for the initial RAFT solution polymerization of MPC in ethanol at 70 °C. After isolation and purification, ^{1}H NMR spectra recorded for the two PMPC precursors in CD_3OD indicated mean DPs of 15 and 26, respectively. More specifically, the integrated signal assigned to the five aromatic dithiobenzoate protons between 7.4 and 8.0 ppm was compared with those corresponding to the six protons of the three oxymethylene proton signals [*i.e.* –COO–C$\underline{H}_2$, C$\underline{H}_2$–O–P and

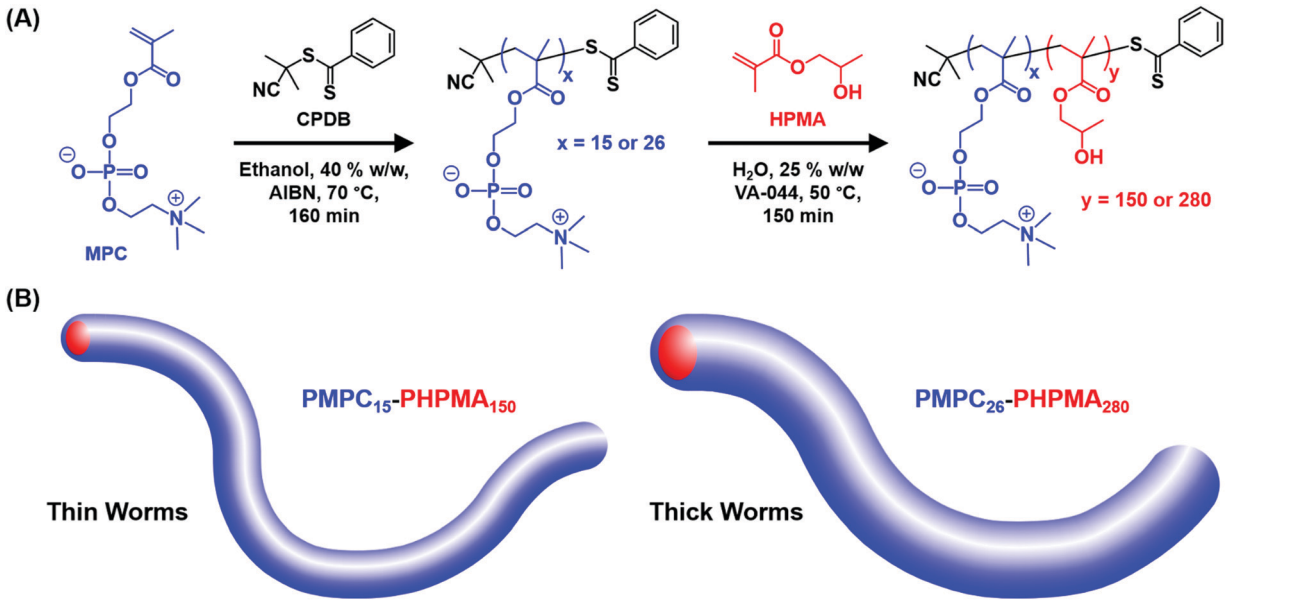

Scheme 1 (A) Reaction scheme for the synthesis of two $PMPC_x$ precursors *via* RAFT solution polymerization of MPC in ethanol using a CPDB RAFT agent at 70 °C, followed by RAFT aqueous dispersion polymerization of HPMA at 50 °C to afford a 25% w/w aqueous dispersion of $PMPC_x$–$PHPMA_y$ diblock copolymer worms. (B) Schematic representation of the relatively thin $PMPC_{15}$–$PHPMA_{150}$ and relatively thick $PMPC_{26}$–$PHPMA_{280}$ worms examined in the present study.

$(H_3C)_3N^+$–CH_2–$C\underline{H}_2$] in the MPC repeat units between 4.0 and 4.5 ppm (see Fig. S1, ESI†). GPC analysis (refractive index detector, 3 : 1 chloroform/methanol eluent) gave low final dispersities ($M_w/M_n < 1.12$), indicating good RAFT control (see Fig. S2, ESI†).

These two relatively well-defined PMPC homopolymer precursors were then chain-extended in turn *via* RAFT aqueous dispersion polymerization of HPMA at 50 °C to afford the desired $PMPC_{15}$–$PHPMA_{150}$ (or $PMPC_{26}$–$PHPMA_{280}$) worms at 25% w/w solids. ^{1}H NMR studies confirmed that the HPMA polymerization proceeded to more than 99% conversion in each case (based on the almost complete disappearance of the vinyl proton signals at 5.7 and 6.2 ppm, see Fig. S1, ESI†). Moreover, high blocking efficiencies were achieved in both cases, with final dispersities of 1.30 and 1.36 being observed for $PMPC_{15}$–$PHPMA_{150}$ and $PMPC_{26}$–$PHPMA_{280}$, respectively. According to a prior study by Li and Armes,[26] the high molecular weight shoulders observed in these chromatograms are attributed to a relatively low level (<0.30 mol%) of dimethacrylate impurity in the HPMA monomer, which inevitably leads to light branching when targeting higher degrees of polymerization for the PHPMA block.[57] As reported by Sugihara *et al.*[15] and Warren *et al.*,[52] the mean cross-sectional diameter of the worms depends on the mean degree of polymerization of the structure-directing hydrophobic PHPMA block. Thus, the $PMPC_{15}$–$PHPMA_{150}$ worms are schematically depicted as being somewhat thinner than the $PMPC_{26}$–$PHPMA_{280}$ worms, see Scheme 1B.

It is perhaps worth emphasizing that it is normally rather difficult to access pure worms *via* PISA because this copolymer morphology typically occupies relatively narrow phase space.[15,25,58] However, the two diblock copolymer compositions were chosen based on our prior knowledge of aqueous PISA formulations. Thus, the $PMPC_{25}$–$PHPMA_x$ phase diagram reported by Sugihara *et al.*[15] was used as a starting point to identify an appropriate target PHPMA DP to afford pure worms at 25% w/w solids. According to TEM analysis (see Fig. 1B), the lowest PHPMA DP to afford a pure worm phase was 280, with a 25% w/w aqueous dispersion of $PMPC_{26}$–$PHPMA_{280}$ worms forming a turbid free-standing gel at 25 °C. According to the master phase diagram reported for the PGMA–PHPMA PISA formulation by Warren *et al.*,[52] it should be possible to use this PHPMA/PMPC molar ratio of 10.8 (*i.e.* 280/26) to estimate the likely diblock copolymer composition that should correspond to pure worms when using shorter PMPC stabilizer blocks. More specifically, for the $PMPC_{15}$ precursor employed in the current study, targeting a mean PHPMA DP of around 162 should produce a pure worm phase. Indeed, this rational approach proved to be fruitful, with well-defined worms being obtained when targeting $PMPC_{15}$–$PHPMA_{150}$. The resulting 25% w/w aqueous dispersion formed a transparent free-standing gel at 25 °C, with the distinctive pink color ascribed to the dithiobenzoate chain-ends (see Fig. 1A). It is perhaps worth mentioning that the thicker $PMPC_{26}$–$PHPMA_{280}$ worms scatter light more strongly, which explains why this 25% w/w aqueous dispersion is relatively turbid, rather than transparent (see Fig. 1B). The formation of soft, free-standing hydrogels in both cases is believed to be the result of multiple inter-worm contacts, as reported by Lovett and co-workers for PGMA–PHPMA worms.[27]

Visual inspection of as-synthesized 25% w/w worm gels stored at (sub-)ambient temperature suggested that neither $PMPC_{15}$–$PHPMA_{150}$ nor $PMPC_{26}$–$PHPMA_{280}$ were thermo-responsive at this relatively high copolymer concentration.

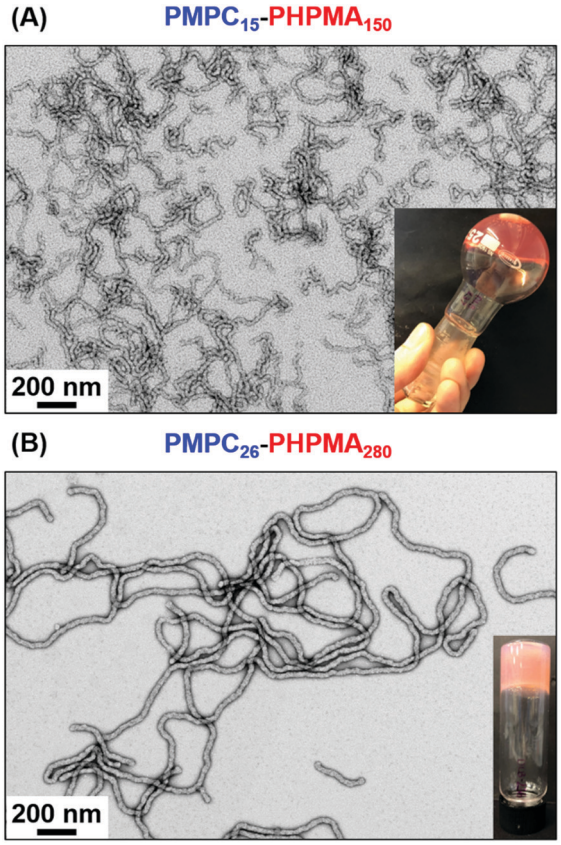

Fig. 1 Representative TEM images recorded for (A) $PMPC_{15}$–$PHPMA_{150}$ worms (number-average cross-sectional diameter = 24.1 ± 1.9 nm) and (B) $PMPC_{26}$–$PHPMA_{280}$ worms (number-average cross-sectional diameter = 31.6 ± 1.8 nm). Inset digital photographs indicate the physical appearance of as-synthesized aqueous dispersions of these 25% w/w diblock copolymer worms, which form either transparent ($PMPC_{15}$–$PHPMA_{150}$) or turbid ($PMPC_{26}$–$PHPMA_{280}$) free-standing gels at 20 °C. These dispersions were diluted to 0.1% w/w using deionized water prior to TEM analysis.

However, serial dilution of these gels led to divergent behavior. Thus, an 18% w/w aqueous dispersion of $PMPC_{15}$–$PHPMA_{150}$ worms formed a transparent free-standing gel at 25 °C but underwent degelation on cooling to 6 °C to afford a free-flowing fluid (Fig. S3, ESI†). According to Blanazs *et al.*, this suggests that a worm-to-sphere morphology transition has occurred.[30] On returning to 25 °C, a tube inversion test confirmed that regelation had occurred (see Fig. S3, ESI†). Dilution of the 25% w/w aqueous dispersion of $PMPC_{26}$–$PHPMA_{280}$ worms to 10% w/w produced a rather soft free-standing, turbid gel at 25 °C. However, in this case no thermoresponsive behavior was observed: degelation did not occur on cooling this gel to 6 °C, even after leaving it to stand for several days at this temperature. This is consistent with observations made by Warren *et al.*, who found that a 10% w/w aqueous $PGMA_{71}$–$PHPMA_{200}$ worm gel underwent degelation on cooling but did not reform a gel on the timescale of the oscillatory rheology experiments.[52] Clearly, PHPMA chains become significantly more hydrophobic as higher DPs are targeted, which is consistent with the thermoresponsive behavior observed by Lovett and co-workers for a series of $PGMA_{43}$–$PHPMA_{175–225}$ vesicles.[34]

Next, variable temperature DLS studies were conducted between 6 and 30 °C on 0.10% w/w aqueous dispersions of $PMPC_{15}$–$PHPMA_{150}$ and $PMPC_{26}$–$PHPMA_{280}$ worms (Fig. 2). DLS is well-suited to characterize isotropic nanoparticles, since the Stokes–Einstein equation assumes a spherical morphology.[59,60] However, useful information can also be obtained for highly anisotropic worms, as reported by Fielding and co-workers.[61] In the present study, the particle size reported by DLS refers to neither the worm length nor the worm cross-sectional diameter (or worm width). Instead, a so-called 'sphere-equivalent' diameter is obtained. Thus, if the worms undergo a morphological transition to form spheres, this can be monitored as a substantial reduction in the 'sphere-equivalent' diameter, even though this parameter only becomes physically meaningful for the final spheres. It is also worth noting that a concomitant reduction in the DLS polydispersity (PDI) would be expected for such a worm-to-sphere transition because the initial worms are relatively polydisperse in length while the final spheres should be more uniform in size.[61] On the other hand, if the initial worms do not undergo a worm-to-sphere transition on cooling, then no change in their sphere-equivalent diameter (or PDI) would be expected.

According to Fig. 2A, the $PMPC_{15}$–$PHPMA_{150}$ worms exhibit a 'sphere-equivalent' diameter of approximately 235 nm (PDI = 0.30) at 30 °C. On cooling to 20 °C, there is an initial gradual reduction to around 220 nm diameter (PDI = 0.30), prior to a much more rapid reduction in apparent size to 37 nm (PDI = 0.21) at 6 °C. These DLS data indicate that a worm-to-sphere transition occurs on cooling. This interpretation is confirmed by TEM analyses of dilute dispersions dried at 25 °C and 6 °C, respectively. Well-defined worms are present at 25 °C while only much smaller spheres are observed at 6 °C. Moreover, on returning to 30 °C, the 'sphere-equivalent' diameter increased only marginally up to 43 nm (PDI = 0.09), indicating that the original worms are not reformed. This is because the 1D stochastic fusion of multiple spheres is very inefficient at the relatively low copolymer concentration required for these DLS experiments, which leads to kinetically-trapped spheres. Similar observations were made by Warren *et al.* for both $PGMA_{54}$–$PHPMA_{140}$ and $PGMA_{71}$–$PHPMA_{200}$ worms.[52] Thus, sufficiently dilute dispersions of worms are characterized by *irreversible* thermoresponsive behavior even if the DP of the PHPMA block has been optimized.

In striking contrast, the 'sphere-equivalent' diameter of the $PMPC_{26}$–$PHPMA_{280}$ worms remains essentially constant at 240–250 nm during a thermal cycle between 6 °C and 30 °C (Fig. 2B). These observations are consistent with TEM images recorded after drying at either 25 °C or 6 °C, which confirm that the original worm morphology remains intact over this temperature range.

DLS studies confirmed that worm reconstitution did not occur at 0.10% w/w copolymer concentration (see Fig. 2A). Accordingly, it was assumed that the nano-objects formed on cooling would become kinetically trapped when diluted to 1.0% w/w at 6 °C, thus allowing SAXS studies to be performed at 25 °C. Thus, $PMPC_{15}$–$PHPMA_{150}$ worms were studied by SAXS

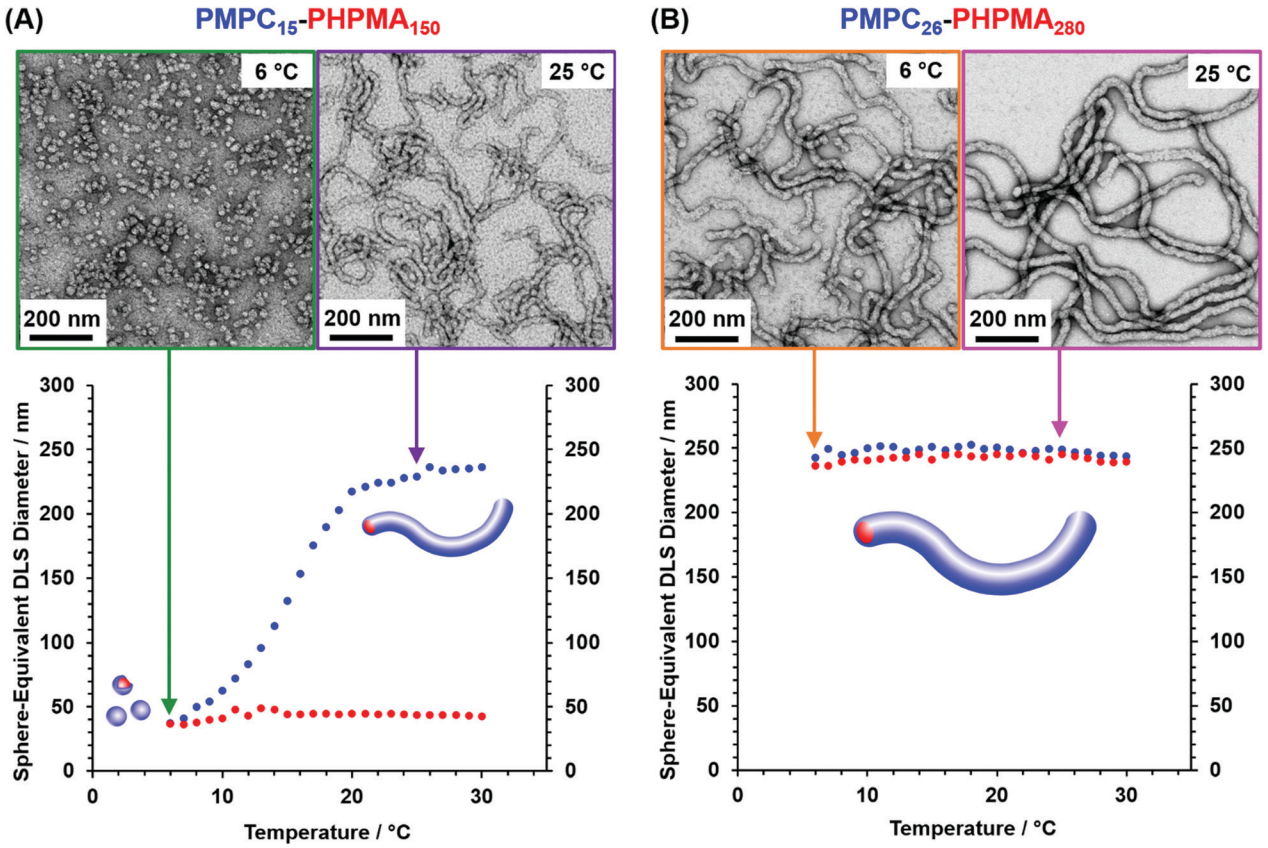

Fig. 2 Temperature dependence of the 'sphere-equivalent' z-average diameter as determined by dynamic light scattering (DLS) studies of 0.10% w/w aqueous dispersions for (A) $PMPC_{15}$–$PHPMA_{150}$ and (B) $PMPC_{26}$–$PHPMA_{280}$ nano-objects. Blue symbols represent the initial cooling cycle and red symbols indicate the subsequent heating cycle. Inset: Representative TEM images (and corresponding schematic cartoons) for the nano-objects recorded after drying at 6 °C and 25 °C. These data confirm that the $PMPC_{15}$–$PHPMA_{150}$ worms undergo an *irreversible* worm-to-sphere transition on cooling to 6 °C, whereas the $PMPC_{26}$–$PHPMA_{280}$ worms remain intact under such conditions.

at 25 °C after sequential dilution of an 18% w/w aqueous dispersion before, during and after a thermal cycle. More specifically, SAXS patterns were recorded for 1.0% w/w aqueous dispersions of (i) the original $PMPC_{15}$–$PHPMA_{150}$ worms at 25 °C, (ii) the $PMPC_{15}$–$PHPMA_{150}$ spheres formed on cooling to 6 °C and (iii) the reconstituted worms obtained on returning the concentrated dispersion to 25 °C, as indicated in the $I(q)$ *vs.* q plots shown in Fig. 3. Each copolymer dispersion was equilibrated at the relevant temperature overnight prior to sequential dilution at that temperature. A gradient of approximately −1 is observed for the initial (red) and the final (green) patterns in the low q region, which is consistent with the presence of highly anisotropic worms.[52] In contrast, the low q gradient is close to zero for the nano-objects diluted at 6 °C, which is consistent with the formation of spheres that become kinetically trapped after dilution. Moreover, these SAXS patterns can be satisfactorily fitted using appropriate scattering models for worm-like micelles (Fig. 3, 25 °C) and spherical micelles (Fig. 3, 6 °C).[52,62,63] Thus, these SAXS data combined with TEM studies confirm that the $PMPC_{15}$–$PHPMA_{150}$ worms exhibit thermoreversible behaviour at 18% w/w (see Fig. S3, ESI†). This is because the stochastic 1D fusion of multiple spheres to form worms is much more efficient at this higher copolymer concentration.

To achieve a satisfactory fit to the SAXS patterns recorded for the original and reconstituted $PMPC_{15}$–$PHPMA_{150}$ worms present at 25 °C, it was necessary to make the Kuhn length (b_w) equal to the worm contour length (L_w) when using the worm-like micelle model. This implies that the worms behave as rigid rods in dilute aqueous solution. Modeling also indicated that the worm core radius (R_w) remained approximately constant before and after being subjected to a thermal cycle (see Table 1). However, a slight increase in the standard deviation for R_w was observed for the reconstituted worms. Furthermore, modeling indicated that the reconstituted worms exhibited slightly shorter L_w values. Unfortunately, there is relatively high experimental uncertainty in the worm contour length. Nevertheless, the contour length obtained from the SAXS fitting is reasonably consistent with the worm length observed in TEM images (see Fig. 1). The number-average core cross-sectional diameter estimated for the original $PMPC_{15}$–$PHPMA_{150}$ worms from TEM analysis (see Fig. 1) was 24.1 ± 1.9 nm, which exceeds the volume-average core cross-sectional diameter ($2R_w$) of 18.8 nm determined by SAXS analysis prior to the thermal cycle.

In principle, TEM should undersize relative to SAXS but the former technique suffers from relatively poor sampling

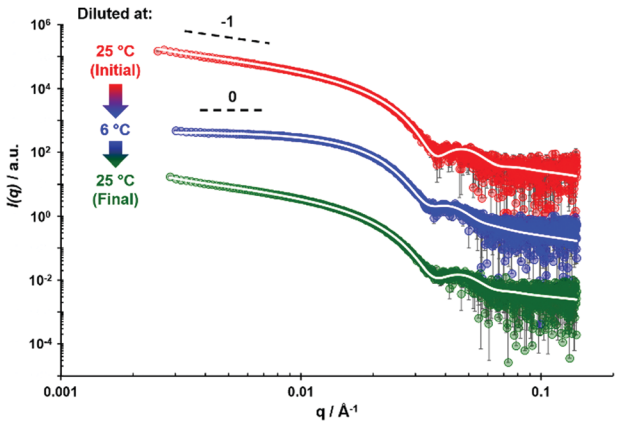

Fig. 3 SAXS patterns recorded at 25 °C for a 1.0% w/w aqueous dispersion of $PMPC_{15}$–$PHPMA_{150}$ nano-objects prepared after dilution of an 18% w/w stock dispersion equilibrated at either 6 or 25 °C. Initial $PMPC_{15}$–$PHPMA_{150}$ nano-objects at 25 °C prior to conducting a thermal cycle (red symbols), after equilibration at 6 °C overnight (blue symbols), and after returning to 25 °C followed by equilibration overnight (green symbols). The white lines indicate the data fits obtained using a worm-like micelle model for the red and green patterns and a spherical micelle model for the blue pattern. Dashed black lines indicate gradients of 0 and −1 and are provided as guidance to the eye. For clarity, the blue and red data sets are offset by factors of 10^2 and 10^4, respectively.

Table 1 Summary of TEM assignments and various SAXS parameters determined from modeling SAXS data recorded for 1.0% w/w aqueous dispersions of $PMPC_{15}$–$PHPMA_{150}$ nano-objects diluted from an 18% w/w stock dispersion that was subjected to a thermal cycle between 25 °C and 6 °C [N.B. R_s and R_w are the sphere and worm core radii respectively, σ_R is the standard deviation in either R_s or R_w, L_w is the worm contour length and b_w is the worm Kuhn length]

	TEM	SAXS				
Thermal history	Morphology assignment	R_s/nm	R_w/nm	σ_R/nm	L_w/nm	b_w[a]/nm
25 °C (initial)	Worms	—	9.4	0.8	283	283
6 °C	Spheres	12.4	—	1.7	—	—
25 °C (final)	Worms	—	9.5	1.1	247	247

[a] To achieve a satisfactory data fit, it was necessary to assume that b_w was equal to L_w, *i.e.* that the worms are relatively inflexible.

statistics. Modeling of the SAXS pattern recorded for the 1.0% w/w aqueous dispersion of $PMPC_{15}$–$PHPMA_{150}$ nano-objects diluted at 6 °C indicated a somewhat larger sphere core radius (R_s) of 12.4 ± 1.7 nm. In principle, this parameter should slightly exceed the worm core radius owing to the subtle change in geometry when multiple spheres fuse together to form cylindrical worms (see Fig. S4, ESI†). Under such circumstances, the worm core radius divided by the sphere core radius should be equal to $\sqrt{2/3}$ or ≈0.82. However, this value should be regarded as an upper limit because the overall surface area is constrained when fusing multiple spheres to form each worm. Thus, reasonably good agreement is observed with the radius ratio of ~0.76 (see Table 1). DLS reports an overall hydrodynamic *z*-average diameter of 37 nm at 6 °C. Using the manufacturer's software, we calculate a corresponding volume-average diameter of 32 nm. Bearing in mind the thickness of the hydrated PMPC stabilizer layer ($2R_g$ = 2.46 nm), the volume-average spherical core diameter ($2R_s$) of 24.8 nm calculated using SAXS is consistent with the latter DLS diameter (since $2R_s + 4R_g$ = 29.7 nm). Furthermore, the increase in the standard deviation of the mean core radius for the spheres formed at 6 °C compared to that of the original worms at 25 °C is consistent with the corresponding TEM images (see Table 1 and Fig. 2).

As predicted by theory,[64] amphiphilic diblock copolymers self-assemble to form nano-objects in selective solvents with core diameters (d) that scale according to the mean DP (N) for the insoluble block.[65–68] These two parameters obey a power law of the form $d = kN^{\alpha}$, where k is a constant related to the Flory–Huggins parameter and α is an exponent that depends on the extent of chain stretching within the nano-object cores.[68] In the context of the present study, such a power law is expected between the worm core diameter ($2R_w$) determined *via* SAXS analysis and the DP of the hydrophobic PHPMA block. Fig. 4 shows the relationship between these two parameters determined for a series of aqueous dispersions of PHPMA–core worms prepared using a non-ionic PGMA stabilizer,[52] various binary mixtures of poly(methacrylic acid) (PMAA) and PGMA,[69] a non-ionic poly[*N*-(2-hydroxypropyl)methacrylamide] (PHPMAC) stabilizer[70] and the two zwitterionic PMPC stabilizers reported herein (see Fig. 3, Table 1, Fig. S5 and Table S1, ESI†). The data fit to this power law returned an exponent of 0.67 (≈2/3), which corresponds to that expected for the strong segregation regime. This indicates that the PHPMA chains located within such worm cores lie between fully stretched (α = 1) and unperturbed random (Gaussian) coils (α = 1/2).[68]

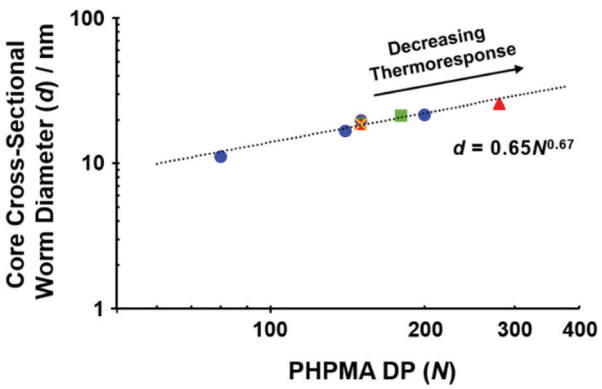

Fig. 4 Scaling relationship between the core cross-sectional diameter, d, of a series of aqueous PHPMA-based worms and the mean DP of the hydrophobic PHPMA block, N. Data were fitted using a power law of the form $d = kN^{\alpha}$, where k is a constant and α is the scaling exponent. From the data fit, α is determined to be 0.67 or ≈2/3. Data reported herein for $PMPC_{15}$–$PHPMA_{150}$ and $PMPC_{26}$–$PHPMA_{280}$ worms (closed red triangles) are plotted with additional data collated from multiple studies: *e.g.* $PGMA_{37}$–$PHPMA_{80}$, $PGMA_{54}$–$PHPMA_{140}$ and $PGMA_{71}$–$PHPMA_{200}$ (closed blue circles),[52] [0.05$PMAA_{85}$ + 0.95$PGMA_{62}$]–$PHPMA_{150}$ (yellow cross),[69] [0.2$PMAA_{85}$ + 0.8$PGMA_{62}$]–$PHPMA_{150}$ (open green diamond),[69] [0.2$PMAA_{37}$ + 0.8$PGMA_{68}$]–$PHPMA_{150}$ (open purple circle)[69] and $PHPMAC_{41}$–$PHPMA_{180}$ (closed green square).[70]

Moreover, α = 0.67 is in fairly good agreement with the exponent of 0.70 calculated by Warren *et al.* for three examples of $PGMA_x$–$PHPMA_y$ worms.[52] However, it is not consistent with the α exponent of unity determined for a series of four $PMPC_{25}$–$PHPMA_y$ worms reported by Sugihara and co-workers.[15] This discrepancy is most likely because TEM was used to estimate the mean worm core diameter rather than SAXS,[15] with the former parameter being much less statistically robust and also prone to drying artifacts. It is perhaps worth mentioning that increasingly weak thermoresponsive character is observed for PHPMA-based worms as the DP of this structure-directing block exceeds 150. This suggests that there is a maximum core diameter for thermoreversible PHPMA-based worms, although further studies would be required to confirm this hypothesis.

The thermoresponsive behavior of the 18% w/w aqueous dispersion of $PMPC_{15}$–$PHPMA_{150}$ worms was subsequently investigated by oscillatory rheology during a 40 °C to 6 °C to 40 °C thermal cycle (Fig. 5A). Preliminary studies enabled the linear viscoelastic regime to be identified (see Fig. S6 and S7, ESI†). G' of the initial worm gel was determined to be approximately 300 Pa at 37 °C. During the cooling cycle, G'' becomes equal to G' at around 17 °C, which corresponds to the CGT. At 6 °C, a free-flowing fluid is obtained ($G' < 1$ Pa). On heating, there is a monotonic increase in G' (albeit with some hysteresis) and a CGT is observed at around 28 °C, with the original bulk modulus eventually being restored at around 40 °C. Similar observations have been reported by Verber *et al.* when subjecting a $PGMA_{54}$–$PHPMA_{150}$ worm gel to a thermal cycle.[29]

The oscillatory rheology data are consistent with TEM and SAXS analysis recorded at lower copolymer concentrations, with both techniques indicating the presence of worms at 25 °C and spheres at 6 °C (see Fig. 3 and Fig. S3, ESI†). Moreover, both TEM and SAXS studies confirm that the worms are reformed on returning to 25 °C, which suggests that the much higher copolymer concentration required for these rheology studies leads to far more efficient 1D sphere-sphere fusion. This is essential for achieving regelation within normal experimental timescales (*i.e.* minutes/hours) because worm reconstitution from spheres is a highly cooperative associative process. In contrast, converting worms into spheres is simply a dissociative process that can proceed rapidly without any impediment. Nevertheless, high copolymer concentrations can retard this transition, as reported by Warren *et al.* for oscillatory rheology studies of 20% w/w aqueous dispersions of $PGMA_{54}$–$PHPMA_{140}$ and $PGMA_{71}$–$PHPMA_{200}$ worms.[52] Based on prior studies by Fielding *et al.*, this latter transition most likely involves a 'budding' mechanism whereby spheres emerge from the worm ends, rather than random worm scission.[61] It is perhaps worth emphasizing that thermoreversible (de)gelation behavior is

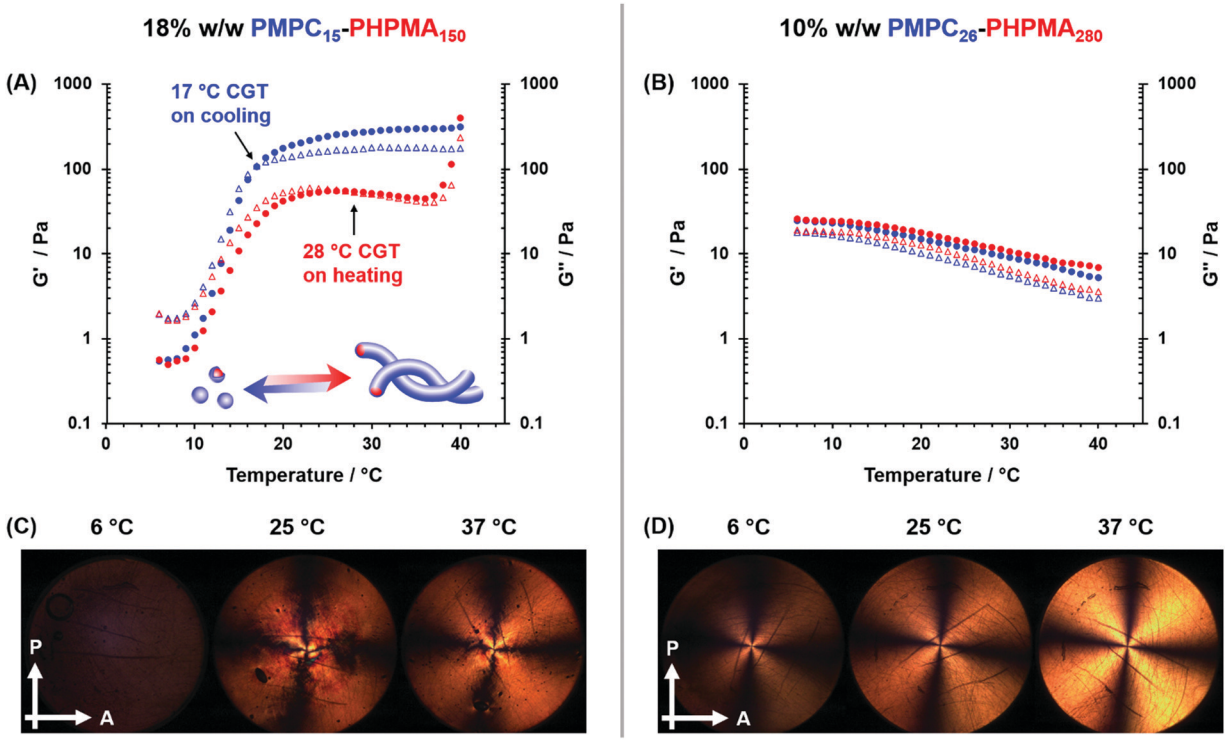

Fig. 5 Variable temperature oscillatory rheology data obtained during cooling (blue symbols) or heating (red symbols) cycles for (A) 18% w/w $PMPC_{15}$–$PHPMA_{150}$ worms and (B) 10% w/w $PMPC_{26}$–$PHPMA_{280}$ worms. (C and D) Corresponding shear-induced polarized light imaging (SIPLI) images recorded at 6, 25 and 37 °C for the same two aqueous copolymer dispersions. G' data are denoted by solid circles and G'' data are indicated by open triangles. For oscillatory rheology, an applied strain of 1.0% and an angular frequency of 1.0 rad s^{-1} were utilized, and a constant shear rate of 1.0 s^{-1} at the sample edge was employed for SIPLI. A thermal equilibration time of 10 min was allowed at each temperature prior to data acquisition for both techniques. The white arrows shown in (C) and (D) indicate the orientation of the polarizer (P) and analyzer (A) planes, respectively.

critical for potential biomedical applications because it enables facile sterilization of such worm gels *via* cold ultrafiltration.[30]

SIPLI studies were conducted at 6, 25 and 37 °C to provide further evidence for the thermally-induced change in copolymer morphology (Fig. 5C). As previously reported by Mykhaylyk *et al.*,[55,56] this relatively new technique enables the presence of isotropic or anisotropic particles to be assessed under shear. After equilibration for 10 min at 6 °C, a dark image was observed for the 18% w/w aqueous dispersion of $PMPC_{15}$–$PHPMA_{150}$ when subjected to an applied shear rate of 1.0 s^{-1}, which indicates the presence of non-birefringent isotropic spheres.[55] At 25 °C, a characteristic Maltese cross pattern is observed; this results from the birefringence produced by *in situ* shear alignment of the highly anisotropic worms. This Maltese cross is retained on further heating to 37 °C, indicating that the worms remain intact at this temperature. These data are fully consistent with the TEM analysis and oscillatory rheology studies conducted on these $PMPC_{15}$–$PHPMA_{150}$ nano-objects. The distorted nature of the Maltese cross observed at 25 and 37 °C in Fig. 5C is attributed to worm entanglements at the relatively high copolymer concentration (18% w/w) used for these SIPLI experiments. A more traditional Maltese cross motif can be obtained by conducting such studies at 10% w/w (see Fig. S8, ESI†).

Variable temperature oscillatory rheology studies were also conducted using a 10% w/w aqueous dispersion of $PMPC_{26}$–$PHPMA_{280}$ worms (see Fig. 5B). On cooling this dispersion from 40 °C to 6 °C, no degelation occurred. In fact, a modest *increase* in gel modulus was observed, with the original gel modulus being restored on returning to 40 °C. Furthermore, SIPLI studies conducted on the same copolymer dispersion revealed a characteristic Maltese cross from 6 °C to 37 °C, suggesting the permanent presence of anisotropic worms (see Fig. 5D). These rheological data are consistent with tube inversion tests, DLS data and TEM analysis, which confirm that $PMPC_{26}$–$PHPMA_{280}$ worms do not exhibit any thermoresponsive behavior over this temperature range.

Serial dilution enabled determination of the CGC at 25 °C. For $PMPC_{15}$–$PHPMA_{150}$ worms, a free-standing transparent gel was obtained at copolymer concentrations of $\geq$15% w/w, whereas a slightly turbid viscous liquid was formed at 12% w/w (see Fig. S9A, ESI†). Gel moduli determined over time indicated that G' was only marginally greater than G'' at approximately 15% w/w. Similar experiments for $PMPC_{26}$–$PHPMA_{280}$ worms indicated a much lower CGC of around 2.5 to 4.0% w/w. However, the latter gels only became free-standing at approximately 10% w/w as judged by the tube inversion test; this is most likely owing to their relatively low gel moduli ($<$10 Pa, see Fig. S9B, ESI†). The CGC is an important parameter in the context of potential biomedical applications, such as 3D cell culture media or long-term cell storage media.[35,37,71] This is because high copolymer concentrations can adversely affect biocompatibility, leading to a reduction in cell viability. Thus, the relatively high CGC observed for the $PMPC_{15}$–$PHPMA_{150}$ worms is not ideal in this context.

However, such cell biology studies require worm gels to be prepared using PBS buffer or a commercial cell culture medium (*e.g. Nutristem*), rather than deionized water. Recently, Sponchioni and co-workers reported substantially different rheological behavior for PEG_{57}–$PHPMA_x$ worm gels in *Nutristem* compared to deionized water.[71] Indeed, to achieve the required thermoresponsive degelation behavior, Sponchioni and co-workers found that the diblock copolymer composition had to be adjusted from PEG_{57}–$PHPMA_{120}$ in water to PEG_{57}–$PHPMA_{65}$ in *Nutristem*.[71] If similar optimization were required for the $PMPC_{15}$–$PHPMA_{150}$ worms to produce the desired rheological performance, reducing the mean DP of the PHPMA block might lead to a significantly lower CGC. Moreover, Sponchioni and co-workers demonstrated that the chemical functionality of the steric stabilizer block is important in determining the fate of naïve embryonic human stem cells.[71] Thus, using a PEG stabilizer block led to cell proliferation, whereas a PGMA stabilizer block induced cell stasis. In this context, it would be fascinating to examine how the PMPC stabilizer block influences stem cell behavior. However, such experiments are likely to require further optimization of the rheological properties of the $PMPC_{15}$–$PHPMA_{150}$ worms reported herein.

Conclusions

Informed by our recent studies of thermoresponsive PGMA–PHPMA diblock copolymer worm gels, which undergo degelation on cooling as a result of a worm-to-sphere transition, we decided to revisit an earlier PMPC–PHPMA worm gel formulation that did not exhibit any thermoresponsive behavior. A rational approach was adopted based on our prior knowledge of various aqueous PISA formulations. More specifically, by targeting a shorter mean degree of polymerization for the structure-directing PHPMA block, we were able to reduce its hydrophobic character and hence introduce the desired thermoresponsive degelation behavior *via* a worm-to-sphere transition when cooling from 25 °C to 6 °C. Moreover, this change in copolymer morphology is reversible: worms are reconstituted on returning to ambient temperature as confirmed by TEM and SAXS studies and the original gel modulus is restored. This should enable facile sterilization *via* cold ultrafiltration and augurs well for potential biomedical applications of such PMPC–PHPMA worm gels, which will be examined in due course. Finally, combining SAXS data previously reported for various PHPMA–core worms with the two types of PMPC–PHPMA worms studied herein enabled examination of the scaling relationship between the worm cross-sectional core diameter and the PHPMA DP. An exponent of 0.67 was observed regardless of the nature of the steric stabilizer block, which is consistent with the strong segregation regime.

Conflicts of interest

There are no conflicts to declare.

Acknowledgements

EPSRC is thanked for a DTA PhD studentship to support D. L. B. and for a four-year EPSRC *Established Career* Particle

Technology Fellowship (EP/003009) for S. P. A. EPSRC is also acknowledged for a capital equipment grant to purchase the Xenocs-Excillum SAXS laboratory beamline (EP/M028437/1).

References

1 B. Charleux, G. Delaittre, J. Rieger and F. D'Agosto, *Macromolecules*, 2012, **45**, 6753–6765.
2 N. J. W. Penfold, J. Yeow, C. Boyer and S. P. Armes, *ACS Macro Lett.*, 2019, **8**, 1029–1054.
3 J. Chiefari, Y. K. B. Chong, F. Ercole, J. Krstina, J. Jeffery, T. P. T. Le, R. T. A. Mayadunne, G. F. Meijs, C. L. Moad, G. Moad, E. Rizzardo, S. H. Thang and C. South, *Macromolecules*, 1998, **31**, 5559–5562.
4 G. Moad, E. Rizzardo and S. H. Thang, *Polymer*, 2008, **49**, 1079–1131.
5 G. Moad, E. Rizzardo and S. H. Thang, *Aust. J. Chem.*, 2012, **65**, 985–1076.
6 S. Perrier, *Macromolecules*, 2017, **50**, 7433–7447.
7 S. L. Canning, G. N. Smith and S. P. Armes, *Macromolecules*, 2016, **49**, 1985–2001.
8 F. D'Agosto, J. Rieger and M. Lansalot, *Angew. Chem., Int. Ed.*, 2020, **59**, 8368–8392.
9 S. Sugihara, M. Sudo and Y. Maeda, *Langmuir*, 2019, **35**, 1346–1356.
10 B. Zhang, X. Lv and Z. An, *ACS Macro Lett.*, 2017, **6**, 224–228.
11 G. Mellot, J. M. Guigner, L. Bouteiller, F. Stoffelbach and J. Rieger, *Angew. Chem., Int. Ed.*, 2019, **58**, 3173–3177.
12 J. Tan, Y. Bai, X. Zhang and L. Zhang, *Polym. Chem.*, 2016, **7**, 2372–2380.
13 O. Nahi, O. J. Cayre, Y. Y. Kim, A. J. Smith, N. J. Warren and F. C. Meldrum, *Chem. Commun.*, 2020, **56**, 7463–7466.
14 J. Tan, D. Liu, X. Zhang, C. Huang, J. He, Q. Xu, X. Li and L. Zhang, *RSC Adv.*, 2017, **7**, 23114–23121.
15 S. Sugihara, A. Blanazs, S. P. Armes, A. J. Ryan and A. L. Lewis, *J. Am. Chem. Soc.*, 2011, **133**, 15707–15713.
16 V. Ladmiral, A. Charlot, M. Semsarilar and S. P. Armes, *Polym. Chem.*, 2015, **6**, 1805–1816.
17 M. Chen, J. W. Li, W. J. Zhang, C. Y. Hong and C. Y. Pan, *Macromolecules*, 2019, **52**, 1140–1149.
18 E. R. Jones, M. Semsarilar, P. Wyman, M. Boerakker and S. P. Armes, *Polym. Chem.*, 2016, **7**, 851–859.
19 D. Zhou, R. P. Kuchel, S. Dong, F. P. Lucien, S. Perrier and P. B. Zetterlund, *Macromol. Rapid Commun.*, 2019, **40**, 1800335.
20 M. J. Rymaruk, C. T. O'Brien, S. L. Brown, C. N. Williams and S. P. Armes, *Macromolecules*, 2020, **53**, 1785–1794.
21 M. J. Derry, L. A. Fielding and S. P. Armes, *Polym. Chem.*, 2015, **6**, 3054–3062.
22 Q. Zhang and S. Zhu, *ACS Macro Lett.*, 2015, **4**, 755–758.
23 N. J. Warren and S. P. Armes, *J. Am. Chem. Soc.*, 2014, **136**, 10174–10185.
24 J. Rieger, *Macromol. Rapid Commun.*, 2015, **36**, 1458–1471.
25 A. Blanazs, A. J. Ryan and S. P. Armes, *Macromolecules*, 2012, **45**, 5099–5107.
26 Y. Li and S. P. Armes, *Angew. Chem., Int. Ed.*, 2010, **49**, 4042–4046.
27 J. R. Lovett, M. J. Derry, P. Yang, F. L. Hatton, N. J. Warren, P. W. Fowler and S. P. Armes, *Chem. Sci.*, 2018, **9**, 7138–7144.
28 Y. Pei, A. B. Lowe and P. J. Roth, *Macromol. Rapid Commun.*, 2017, **38**, 1600528.
29 R. Verber, A. Blanazs and S. P. Armes, *Soft Matter*, 2012, **8**, 9915–9922.
30 A. Blanazs, R. Verber, O. O. Mykhaylyk, A. J. Ryan, J. Z. Heath, C. W. I. Douglas and S. P. Armes, *J. Am. Chem. Soc.*, 2012, **134**, 9741–9748.
31 V. J. Cunningham, L. P. D. Ratcliffe, A. Blanazs, N. J. Warren, A. J. Smith, O. O. Mykhaylyk and S. P. Armes, *Polym. Chem.*, 2014, **5**, 6307–6317.
32 N. J. Warren, J. Rosselgong, J. Madsen and S. P. Armes, *Biomacromolecules*, 2015, **16**, 2514–2521.
33 L. P. D. Ratcliffe, K. J. Bentley, R. Wehr, N. J. Warren, B. R. Saunders and S. P. Armes, *Polym. Chem.*, 2017, **8**, 5962–5971.
34 J. R. Lovett, N. J. Warren, S. P. Armes, M. J. Smallridge and R. B. Cracknell, *Macromolecules*, 2016, **49**, 1016–1025.
35 I. Canton, N. J. Warren, A. Chahal, K. Amps, A. Wood, R. Weightman, E. Wang, H. Moore and S. P. Armes, *ACS Cent. Sci.*, 2016, **2**, 65–74.
36 D. E. Mitchell, J. R. Lovett, S. P. Armes and M. I. Gibson, *Angew. Chem., Int. Ed.*, 2016, **55**, 2801–2804.
37 K. A. Simon, N. J. Warren, B. Mosadegh, M. R. Mohammady, G. M. Whitesides and S. P. Armes, *Biomacromolecules*, 2015, **16**, 3952–3958.
38 S. I. Yusa, K. Fukuda, T. Yamamoto, K. Ishihara and Y. Morishima, *Biomacromolecules*, 2005, **6**, 663–670.
39 T. Ueda, H. Oshida, K. Kurita, K. Ishihara and N. Nakabayashi, *Polym. J.*, 1992, **24**, 1259–1269.
40 K. Ishihara, H. Nomura, T. Mihara, K. Kurita, Y. Iwasaki and N. Nakabayashi, *J. Biomed. Mater. Res.*, 1998, **39**, 323–330.
41 S. Monge, B. Canniccioni, A. Graillot and J. J. Robin, *Biomacromolecules*, 2011, **12**, 1973–1982.
42 K. Ishihara, *J. Biomed. Mater. Res., Part A*, 2019, **107**, 933–943.
43 A. L. Lewis, *Colloids Surf., B*, 2000, **18**, 261–275.
44 Y. Iwasaki and K. Ishihara, *Anal. Bioanal. Chem.*, 2005, **381**, 534–546.
45 H. Kitano, M. Imai, T. Mori, M. Gemmei-Ide, Y. Yokoyama and K. Ishihara, *Langmuir*, 2003, **19**, 10260–10266.
46 T. Goda and K. Ishihara, *Expert Rev. Med. Devices*, 2006, **3**, 167–174.
47 A. L. Lewis, T. A. Vick, A. C. M. Collias, L. G. Hughes, R. R. Palmer, S. W. Leppard, J. D. Furze, A. S. Taylor and P. W. Stratford, *J. Mater. Sci.: Mater. Med.*, 2001, **12**, 865–870.
48 K. Ishihara, *Sci. Technol. Adv. Mater.*, 2000, **1**, 131–138.
49 T. A. Snyder, H. Tsukui, S. Kihara, T. Akimoto, K. N. Litwak, M. V. Kameneva, K. Yamazaki and W. R. Wagner, *J. Biomed. Mater. Res., Part A*, 2007, **81**, 85–92.
50 T. Moro, Y. Takatori, K. Ishihara, T. Konno, Y. Takigawa, T. Matsushita, U. I. L. Chung, K. Nakamura and H. Kawaguchi, *Nat. Mater.*, 2004, **3**, 829–836.

51 Y. Iwasaki and K. Ishihara, *Sci. Technol. Adv. Mater.*, 2012, **13**, 064101.
52 N. J. Warren, M. J. Derry, O. O. Mykhaylyk, J. R. Lovett, L. P. D. Ratcliffe, V. Ladmiral, A. Blanazs, L. A. Fielding and S. P. Armes, *Macromolecules*, 2018, **51**, 8357–8371.
53 R. Spelat, F. Ferro, P. Contessotto, N. J. Warren, G. Marsico, S. P. Armes and A. Pandit, *Mater. Today Bio*, 2020, **5**, 100040.
54 J. Ilavsky and P. R. Jemian, *J. Appl. Crystallogr.*, 2009, **42**, 347–353.
55 O. O. Mykhaylyk, N. J. Warren, A. J. Parnell, G. Pfeifer and J. Laeuger, *J. Polym. Sci., Part B: Polym. Phys.*, 2016, **54**, 2151–2170.
56 O. O. Mykhaylyk, *Soft Matter*, 2010, **6**, 4430–4440.
57 I. Bannister, N. C. Billingham, S. P. Armes, S. P. Rannard and P. Findlay, *Macromolecules*, 2006, **39**, 7483–7492.
58 J. Tan, D. Liu, Y. Bai, C. Huang, X. Li, J. He, Q. Xu, X. Zhang and L. Zhang, *Polym. Chem.*, 2017, **8**, 1315–1327.
59 C. M. Maguire, M. Rösslein, P. Wick and A. Prina-Mello, *Sci. Technol. Adv. Mater.*, 2018, **19**, 732–745.
60 S. E. Harding, D. B. Sattelle and V. A. Bloomfield, *Laser light scattering in biochemistry*, The Royal Society of Chemistry, Cambridge, 1992.
61 L. A. Fielding, J. A. Lane, M. J. Derry, O. O. Mykhaylyk and S. P. Armes, *J. Am. Chem. Soc.*, 2014, **136**, 5790–5798.
62 J. S. Pedersen, *J. Appl. Crystallogr.*, 2000, **33**, 637–640.
63 J. S. Pedersen and P. Schurtenberger, *Macromolecules*, 1996, **29**, 7602–7612.
64 F. S. Bates and G. H. Fredrickson, *Annu. Rev. Phys. Chem.*, 1990, **41**, 525–557.
65 J. Noolandi and K. M. Hong, *Macromolecules*, 1983, **16**, 1443–1448.
66 S. Förster, M. Zisenis, E. Wenz and M. Antonietti, *J. Chem. Phys.*, 1996, **104**, 9956–9970.
67 P. Dalhaimer, H. Bermudez and D. E. Discher, *J. Polym. Sci., Part B: Polym. Phys.*, 2004, **42**, 168–176.
68 G. Battaglia and A. J. Ryan, *J. Am. Chem. Soc.*, 2005, **127**, 8757–8764.
69 L. A. Fielding, C. T. Hendley, E. Asenath-Smith, L. A. Estroff and S. P. Armes, *Polym. Chem.*, 2019, **10**, 5131–5141.
70 L. P. D. Ratcliffe, M. J. Derry, A. Ianiro, R. Tuinier and S. P. Armes, *Angew. Chem., Int. Ed.*, 2019, **58**, 18964–18970.
71 M. Sponchioni, C. T. O'Brien, C. Borchers, E. Wang, M. N. Rivolta, N. J. W. Penfold, I. Canton and S. P. Armes, *Chem. Sci.*, 2020, **11**, 232–240.

